

SOFT X-RAY SELF-SEEDING SIMULATION METHODS AND THEIR APPLICATION FOR LCLS

Svitozar Serkez

Deutsches Elektronen-Synchrotron (DESY), Hamburg, Germany

Jacek Krzywinski, Yuantao Ding, Zhirong Huang

SLAC, Menlo Park, California, USA

Abstract

Self-seeding is a promising approach to significantly narrow the Self-Amplified Spontaneous Emission (SASE) bandwidth of XFELs to produce nearly transform-limited pulses. We study radiation propagation through the grating monochromator installed at Linac Coherent Light Source (LCLS). The monochromator design is based on a toroidal Variable Line Spacing (VLS) grating working at a fixed incidence angle mounting without an entrance slit. It covers the spectral range from 500 eV to 1000 eV. The optical system was studied using wave optics method to evaluate the performance of the self-seeding scheme. Our wave optics analysis takes into account the finite size of the coherent source, third-order aberrations and height error of the optical elements. Wave optics is the only method available, in combination with FEL simulations, to simulate performance of the monochromator without exit slit. Two approaches for time-dependent simulations are presented, compared and discussed.

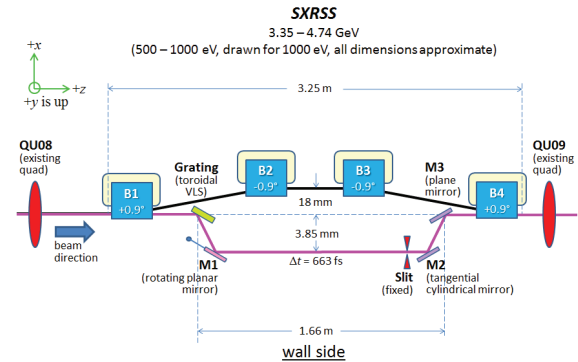


Figure 1: The compact soft x-ray self-seeding system to be located in U9. The grating is a toroidal VLS grating, M1 is a rotating plane mirror, M2 a tangential cylindrical mirror, and M3 a plane mirror used to steer the beam. Adapted from [13].

LCLS SOFT X-RAY SELF-SEEDING SETUP LAYOUT

The overall self-seeding setup consists of three parts: the SASE undulator, the self-seeding grating monochromator and the output seeded undulator in which the monochromatic seed signal is being amplified. The seeded undulator consists of two sections. The first section is composed by an uniform undulator, and the second section - by a tapered undulator. The transform-limited seed pulse is exponentially amplified passing through the first uniform part of the seeded undulator. Finally, in the second part of the seeded undulator the monochromatic FEL output is enhanced after saturation.

The Soft X-ray Self-Seeding (SXRSS) monochromator for LCLS was introduced in [13] and is based on a toroidal variable-line-spacing (VLS) grating, a steering plane mirror, a slit, a spherical mirror and another plane mirror (Fig. 1).

The toroidal VLS grating is illuminated by a SASE FEL radiation produced by the SASE undulator with the source in undulator sections 7 or 8 (depends on set-up). Transverse coherence of a SASE FEL allows one to avoid installation of an entrance slit. The plane mirror M1 is used to steer the certain wavelength of an angularly dispersed radiation to the slit. The spherical mirror M2 re-images the radiation from the slit position to the re-imaging point at the entrance to the seeded undulator. The plane mirror M3 reflects the radiation to the seeded undulator, allowing two additional

INTRODUCTION

Self-seeding is a promising approach to significantly narrow the SASE bandwidth and to produce a nearly transform-limited pulses [1]- [10]. Recently a soft X-ray Self-seeding setup was installed in LCLS [11]- [15] and is currently under commissioning [16].

In general, a self-seeding setup consists of two undulators separated by a photon monochromator and an electron bypass, normally a four-dipole chicane (see Fig. 1). Both undulators are resonant at the same radiation wavelength. The SASE radiation generated by the first undulator (SASE undulator) passes through the narrow-band monochromator. A monochromatic pulse is created, which is used as a coherent seed in the second undulator (seeded undulator). Chromatic dispersion effect in the bypass chicane smears out the microbunching in the electron bunch produced by the SASE lasing in the SASE undulator. The electrons and the monochromatized photon beam are recombined at the entrance of the seeded undulator, and the radiation is amplified by the electron bunch until saturation is reached. The required seed power at the beginning of the seeded undulator must dominate over the shot noise power within the gain bandpass, which is order of a kW in the soft X-ray range.

degrees of freedom for an overlap of the electron beam and the monochromatic radiation.

OPTICS MODELING

In order to simulate transformation of the radiation after passing the entire optical system of the monochromator, we model an effect of a different optical components. Propagation is carried out through an every component sequentially, as the radiation approaches them. Drift spaces are simulated in between. Simulation is based on a single frequency beam propagation method. Fresnel propagator is used to simulate drift spaces (e.g. [17]) and phase shifter method - to simulate optical elements. [18]. A phase-shifter model is used to simulate a focusing effect of the toroidal grating, M2 mirror and contribution of height errors of an optical element surfaces. This model implies an introduction of a shift to a phase of radiation $\Delta\Phi(x, y)$. This shift is dependent on a transverse position at radiation distribution and only changes the phase of the reflected beam without changing its amplitude. It allows one to change the wavefront curvature, therefore field behavior after propagation. In practice, $\Delta\Phi$ represents the deformation of the wavefront in propagation direction divided by the wavelength.

Free Space Propagation

Let's consider electric field in a space-time domain $\vec{E}(t, x, y)$ expressed in Cartesian coordinate system. In this domain radiation is exported from the FEL simulation code GENESIS [19]. Applying temporal and frequency Fourier transforms one obtains the electric field in inverse space-frequency domain - $\vec{E}(\omega, k_x, k_y)$.

Radiation distribution with frequency $\omega = k_0 c$ at a distance z after free space propagation one can calculate with a spatial-frequency response function in paraxial approximation [17]:

$$H(\omega, k_x, k_y, z) \simeq \exp[ik_0 z] \exp\left[-\frac{iz}{2k_0}(k_x^2 + k_y^2)\right],$$

$$\vec{E}(\omega, k_x, k_y, z) = \vec{E}(\omega, k_x, k_y, 0) \cdot H(\omega, k_x, k_y, z). \quad (1)$$

Grating Modeling

We model the toroidal VLS grating as a sum of independent contributions of a sagittal focusing element, a tangential focusing element, C_{12} and C_{30} aberrations, a surface height error and a wavelength-dependent tilt, responsible for angular dispersion. Also, asymmetry of incidence and diffraction angles has to be accounted. Since angles of incidence and diffraction from a grating are not equal, a radiation is re-sized transversely in dispersive dimension by the grating asymmetry parameter $b = \sin \theta_i / \sin \theta_d$.

Radiation distribution at any optical component in our simulation is modified by a phase-shifter in the following way:

$$\vec{E}(\omega, x, y) = \vec{E}_0(\omega, x, y) \exp[i\Delta\Phi(x, y, \dots)]. \quad (2)$$

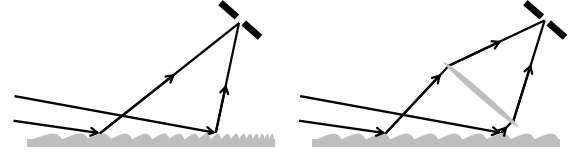


Figure 2: Schematic diagram of a VLS grating element. The VLS grating (left) is represented by a contribution of a planar grating with fixed line spacing and a thin lens (right).

Here $\Delta\Phi$ is a phase shift that depends on various parameters, depending on effect we want to model.

Tangential and sagittal curvatures of the toroidal grating act as an independent cylindrical lenses with the following curvature-determined focal lengths:

$$f_{tang}^{curv} = \frac{R_{tang}}{1/\theta_d + \theta_i/\theta_d^2},$$

$$f_{sag}^{curv} = \frac{R_{sag}}{\theta_i + \theta_d}. \quad (3)$$

Here R_{tang} and R_{sag} are tangential and sagittal radii of curvature, θ_i and θ_d are incidence and diffraction angles respectively. Eq. 3 shows that focal lengths are wavelength-dependent, since $\theta_d = \arccos(\cos \theta_i - \lambda D_0)$, accordingly to the grating equation.

Beside a toroidal curvature, the grating has a variable line spacing with the following line density: $D = D_0 + D_1 l + D_2 l^2$ [lines/mm], where l is a length along the grating.

The VLS focusing contribution may be modeled via introduction of another focusing element in a tangential plane [20] with the following focal length [21]:

$$f_{tang}^{vls} = \frac{\sin^2 \theta_d}{D_1 \lambda}. \quad (4)$$

Toroidal reflecting surfaces introduce aberrations. Two most important contributions are determined by twofold astigmatism and coma aberrations with C_{12} and C'_{30} coefficients correspondingly [22], [21]:

$$C_{12} = -\frac{1}{2} \left(-\frac{\sin \theta_i \cos \theta_i}{R_{sag} z_1} + \frac{\cos \theta_i}{z_1^2} + \frac{\sin \theta_d \cos \theta_d}{R_{sag} z_2} - \frac{\cos \theta_d}{z_2^2} \right),$$

$$C'_{30} = \frac{\lambda n D_2}{3} + \left(\frac{\sin^2 \theta_i}{z_1} - \frac{\sin \theta_i}{R_{tang}} \right) \frac{\cos \theta_i}{2z_1} - \left(\frac{\sin^2 \theta_d}{z_2} - \frac{\sin \theta_d}{R_{tang}} \right) \frac{\cos \theta_d}{2z_2}. \quad (5)$$

Here z_1 and z_2 are distances from an optical element [grating] to an object and an image correspondingly and n is a diffraction order which our case is equal to unity. The quadratic VLS coefficient D_2 introduces a phase shift, that is proportional to x^3 , therefore it is used to compensate the effect of C'_{30} aberration term.

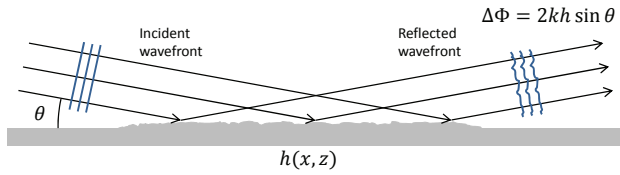


Figure 3: Thin-shifter-like effect of surface height errors for a small mean square of surface displacement, concept adapted from [23].

Aberrations are eliminated when $C'_{30} = 0$ and $C_{12} = 0$ criteria are fulfilled.

In order to simulate time-dependent phenomena of the grating's resolving power one needs to take into account grating dispersion. We propose to induce a wavefront tilt, according to an angular dispersion of the grating. Each wavelength is reflected from the grating at a different angle. Having an ensemble of wavelengths we can choose a principle ray wavelength λ that will propagate downstream with no wavefront tilt. Other wavelengths will propagate from the grating at a certain angles from the principle ray, determined by a grating angular dispersion, e.g. $\lambda_0 + \Delta\lambda$ will be tilted by:

$$\Delta\theta = \frac{\Delta\lambda D_0}{\theta_d}, \quad (6)$$

where $\theta_d = \arccos(\cos \theta_i - \lambda D_0)$.

In this case a linear phase tilt should be applied with respect to the principal ray frequency ω_0 :

$$\Delta\Phi(x, y, \omega_0, \Delta\omega) = -\frac{2\pi x \Delta\theta}{\lambda_0} = \frac{2\pi x \Delta\omega D_0}{\omega_0 \theta_d}. \quad (7)$$

Finally, cumulative effect of the grating modeling may be written as

$$\begin{aligned} \vec{E}(\omega, x, y) &= \vec{E}_0(\omega, x, y) \exp[i\Delta\Phi], \\ \Delta\Phi &= k \left(-\frac{f_{iang} x^2 - f_{sag} y^2}{2} + \frac{C_{30} x^3}{\theta_d^3} \right. \\ &\quad \left. + \frac{C_{12} x y^2}{\theta_d} + \frac{2\pi x \Delta\omega D_0}{k \omega \theta_d} \right). \end{aligned} \quad (8)$$

Focusing with Mirrors

In SXRSS setup another optical element, where tangential curvature is present is M2 mirror. In this case simulation is similar to the grating, but D_0 , D_1 and D_2 VLS coefficients are equal to zero, $\theta_i = \theta_d$, and no field resizing should be applied.

Mirror Surface Height Errors Simulation

A very important issue is to keep track of the radiation quality degradation caused by reflections from optical elements with imperfect surfaces. Phase-shifter model was used to simulate this effect, [23] (see Fig. 3). The height error

δh on an optical surface will perturb the radiation wavefront with a phase shift $\Delta\Phi$ in the following way:

$$\Delta\Phi = \frac{4\pi\delta h}{\lambda} \sin \theta, \quad (9)$$

where θ is the radiation's angle of incidence with respect to the surface. In the case of a grating, the phase shift can be expressed in terms of incidence and diffraction angles:

$$\Delta\Phi = 2\pi(\sin \theta_i + \sin \theta_d) \frac{\delta h}{\lambda}. \quad (10)$$

SIMULATION DETAILS AND APPROACHES

SASE FEL distribution at the end of the last section of SASE undulator is obtained with the GENESIS software. It is dumped in a space-time domain. We apply a temporal Fourier transform, and once obtained the radiation distribution in a space-frequency domain, transverse distributions for an every calculated discrete frequency are treated separately. We apply a Fresnel propagator from Eq. (1) with z equal to a distance between the end of the undulator and the hit point at the grating. The phase shifter, described in Eq. (8) is used to simulate focusing of the beam by the toroidal VLS grating. Tilt is introduced accordingly to a difference $\Delta\omega$ between the frequency being currently propagated and the frequency that is chosen to be a principle ray of dispersed radiation (Eq. 7). After the grating, beam is propagated to M1 position, then to M2 mirror with multiplication by it's focusing phase shifter, then to M3 following with the final propagation to the entrance of the seeded undulator. At the every reflecting optical element a height error phase shifter (Eq. 10) with a certain height error profile is applied. This propagation is applied for an every frequency, therefore we may obtain a space-time domain of the dispersed radiation (Fig. 4) with an inverse temporal Fourier transform and use it as a seed in a GENESIS simulations of the seeded undulator. We call this approach the "direct" one.

On the other hand, one may characterize the monochromator performance by calculation of it's instrumental function (Fig. 5). It can be achieved by propagation of a certain typical transverse distribution with a different tilts that correspond to a different wavelengths (Eq. 7). At the entrance to the seeded undulator these distributions will have a varying transverse offset and after amplification simulation in linear mode one will obtain an amplified power as a function of a wavelength. If that power is normalized by the input coupling factor at 1-to-1 imaging from the end of the SASE undulator to the entrance to the seeded undulator it can be interpreted as an instrumental function of the monochromator at a given set-up (wavelength, FEL gain length, etc.) It allows one to avoid propagation of every pulse by only multiplying radiation distribution in space-frequency domain at the end of the SASE undulator by the instrumental function of monochromator. This way one obtains the radiation distribution at

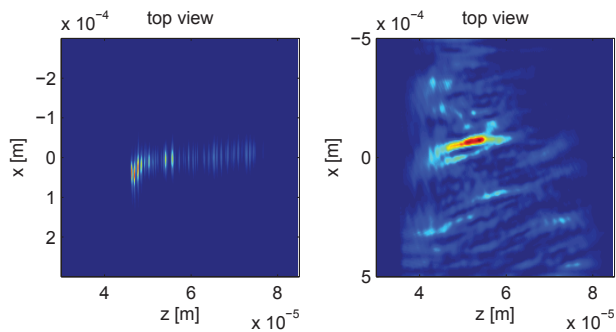


Figure 4: An example of dispersive projection of the radiation distribution in a space-time domain for the FEL pulse before the monochromator (left) and the dispersed radiation distribution after the monochromator (right). Here “x” is a dispersive dimension, and “z” is a dimension along the pulse propagation direction.

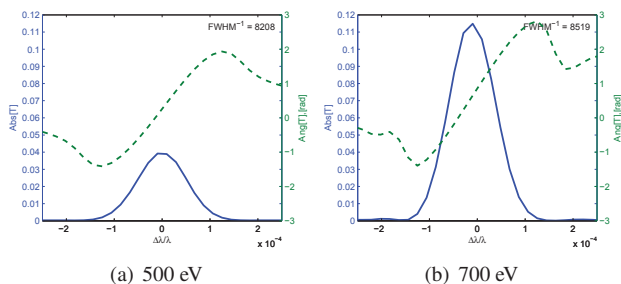


Figure 5: An example of monochromator instrumental functions for a different photon energies. Physical slit is not inserted. An inverse full width at half maximum can be interpreted as an effective resolving power of the monochromator.

the entrance to the seeded undulator. We call this approach the “phenomenological” one. The phase of the instrumental function is obtained with Kramers-Kronig relations (this approach was also used for Hard X-Ray Self Seeding (HXRSS) setup simulation in e.g. [8], [9]). In this case the transverse distribution of the radiation doesn’t change after passing the undulator, which does not correspond to reality, but this distribution is amplified in seeded undulator the same way as one obtained with “direct” approach (Fig. 6) yielding the same radiation properties after amplification (Fig. 7).

CONCLUSIONS

This article describes a way to numerically simulate a propagation of the radiation through the optical system of the Soft X-ray Self Seeding Monochromator. The propagated field is used as a seed for a GENESIS simulations downstream the monochromator allowing one to investigate the FEL beamline performance after the monochromator installation. The monochromator’s optical elements are represented as a transverse phase shifters, allowing to

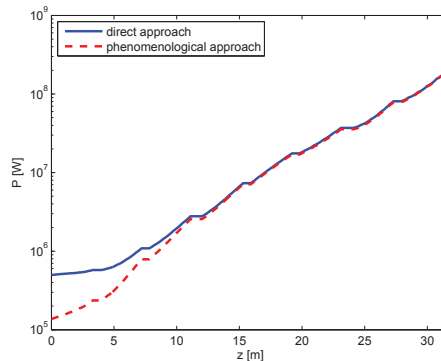


Figure 6: Power of the radiation in the seeded undulator. The radiation was propagated through the seeded undulator with the direct (solid line) and the phenomenological (dashed line) approaches. Pulse energy is 1000 eV.

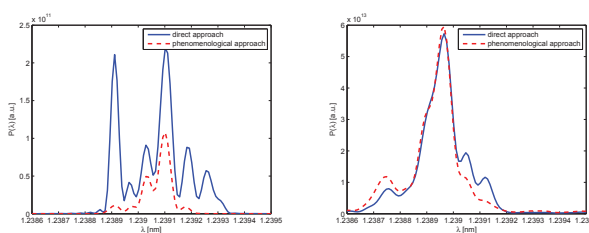


Figure 7: Spectra of the radiation at the seeded undulator entrance (left figure) and exit (right figure). The radiation was propagated through the seeded undulator with the direct (solid line) and the phenomenological (dashed line) approaches. Pulse energy is 1000 eV.

modify the radiation wavefront accordingly to curvatures, positions and height errors of mirrors and aberrations introduced by them. Propagation of the radiation between optical elements is done with Fresnel propagator. The monochromator radiation transport simulation allows one to study the monochromator performance in the beamline, such as effective resolving power of the monochromator without the exit slit, the input coupling factor, or effectiveness of a tapering. Two approaches described above allow one to fill the gap in numerical simulations of FEL performance with SXRSS monochromator.

Based on simulations, we found that resolving power of the LCLS SXRSS monochromator operating without the exit slit varies from 5400 to 8500, that is close to resolving power with $3\mu\text{m}$ exit slit inserted [13]. Resolving power along with input coupling factor are affected by the choice of source position in the SASE undulator. Surface height errors of installed optics have shown no significant effect on the monochromator performance. More detailed study is to be published [24].

REFERENCES

- [1] J. Feldhaus et al., "Possible application of X-ray optical elements for reducing the spectral bandwidth of an X-ray SASE FEL" *Optics. Comm.*, vol. 140, pp. 341-352, 1997.
- [2] E. Saldin et al., "X-ray FEL with a meV bandwidth", *NIM, ser. A*, vol. 475, pp. 357-362, Dec. 2001.
- [3] E. Saldin et al., "Optimization of a seeding option for the VUV free electron laser at DESY", *NIM, ser. A*, vol. 445, pp. 178-182, May 2000.
- [4] R. Treusch et al., "The seeding project for the FEL in TTF phase II", *DESY Ann. report*, 2001.
- [5] A. Marinelli et al., "Comparative study of nonideal beam effects in high gain harmonic generation and self-seeded free electron lasers", *Phys. Rev. ST Accel. Beams*, vol. 13, p. 070701, Jul 2010.
- [6] G. Geloni et al., "Scheme for generation of highly monochromatic X-rays from a baseline XFEL undulator", *DESY 10-033*, 2010.
- [7] Y. Ding et al., "Two-bunch self-seeding for narrow-bandwidth hard x-ray free-electron lasers" *Phys.Rev.ST Accel.Beams*, vol. 13, p. 060703, 2010.
- [8] G. Geloni et al., "A simple method for controlling the line width of SASE X-ray FELs", *DESY 10-053*, 2010.
- [9] G. Geloni et al., "Cost-effective way to enhance the capabilities of the LCLS baseline", *DESY 10-133* 2010.
- [10] G. Geloni et al., "A novel Self-seeding scheme for hard X-ray FELs", *Journal of Modern Optics*, vol. 58, issue 16, pp. 1391-1403, DOI:10.1080/09500340.2011.586473, 2011.
- [11] Y. Feng et al., "Optics for Self-Seeding Soft X-ray FEL Undulators", *Proc. 34th Int. Free-Electron Laser Conf.*, Malmo, Sweden, 2010, TUPB10.
- [12] Y. Feng et al., "Compact Grating Monochromator Design for LCLS-I Soft X-ray Self-Seeding", Available: https://slacportal.slac.stanford.edu/sites/lcls_public/lcls_ii/Lists/LCLS_II_Calendar/Physics_Meetings.aspx, May 2011 and <https://sites.google.com/a/lbl.gov/realizing-the-potential-of-seeded-fels-in-the-soft-x-ray-regime-workshop/talks>, Oct. 2011.
- [13] Y. Feng et al., "System design for self-seeding the LCLS at soft X-ray energies", *Proc. 34th Int. Free-Electron Laser Conf.*, Nara, Japan, 2012, TUOB10.
- [14] D. Cocco et al. "The optical design of the soft x-ray self seeding at LCLS ", *Proc. SPIE*, vol. 8849, p. 88490A, doi:10.1117/12.2024402, Available: <http://dx.doi.org/10.1117/12.2024402>, Sep. 2013.
- [15] D. Cocco, private communication, 2013.
- [16] D. Ratner, "Soft X-ray Self-Seeding Setup and Results at LCLS", talk at this conference: 36th Int. Free-Electron Laser Conf., Basel, 2014, to be published.
- [17] T. Poon and T. Kim, "Engineerig optics in Matlab", *World Scientific*, 2006, pp. 73-78.
- [18] D. G. Voelz, "Computational Fourier Optics: A Matlab Tutorial", *SPIE Press*, Washington, 2011, pp. 89-98.
- [19] S. Reiche et al., "GENESIS 1.3: a fully 3D time-dependent FEL simulation code", *Nucl. Instr. and Meth., ser. A*, vol. 429, pp. 243-248, 1999.
- [20] M. Itou et al., "Soft x-ray monochromator with a varied-space plane grating for synchrotron radiation: design and evaluation", *Applied Optics*, vol. 28, pp. 146-153, 1989.
- [21] S. Serkez et al., "Grating monochromator for soft X-ray self-seeding the European XFEL", *DESY 13-040*, Available: <http://arxiv.org/abs/1303.1392>, 2013.
- [22] T. Harada et al., "Design of a high-resolution extreme-ultraviolet imaging spectrometer with aberration-corrected concave gratings", *Applied optics*, vol. 37, pp. 6803-6810, 1998.
- [23] A. Barty et al., "Predicting the coherent X-ray wavefront focal properties at the Linac Coherent Light Source (LCLS) X-ray free electron laser", *Optics Express*, vol. 17, pp. 15508-15519, 2009.
- [24] S. Serkez et al., "Soft X-ray Self-Seeding simulation methods and their application for LCLS", to be published.